Properties of arsenic–implanted Hg$_{1-x}$Cd$_x$Te MBE films

Igor I. Izhnin[1,2], *Alexandr V.* Voitsekhovskii[2], *Alexandr G.* Korotaev[2], *Olena I.* Fitsych[3], *Oleksandr Yu.* Bonchyk[4], *Hrygory V.* Savytskyy[4], *Karim D.* Mynbaev[5,6,*], *Vasilii S.* Varavin[7], *Sergey A.* Dvoretsky[7], *Maxim V.* Yakushev[7], *Rafal* Jakiela[8], and *Malgorzata* Trzyna[9]

[1]Scientific Research Company "Carat", 79031 Lviv, Ukraine
[2]National Research Tomsk State University, 634050 Tomsk, Russia
[3]Hetman Petro Sahaidachny National Army Academy, 79012 Lviv, Ukraine
[4]Ya.S. Pidstryhach Institute for Applied Problems of Mechanics and Mathematics NASU, 79060 Lviv, Ukraine
[5]Ioffe Institute, 194021 Saint-Petersburg, Russia
[6]ITMO University, 197101 Saint-Petersburg, Russia
[7]Rzhanov Institute of Semiconductor Physics, 630090 Novosibirsk, Russia
[8]Institute of Physics, Polish Academy of Sciences, 02-668 Warsaw, Poland
[9]Faculty of Mathematics and Natural Sciences, University of Rzeszow, 35-310 Rzeszow, Poland

Abstract. Defect structure of arsenic-implanted Hg$_{1-x}$Cd$_x$Te films (x=0.23–0.30) grown with molecular-beam epitaxy on Si substrates was investigated with the use of optical methods and by studying the electrical properties of the films. The structural perfection of the films remained higher after implantation with more energetic arsenic ions (350 keV vs 190 keV). 100%-activation of implanted ions as a result of post-implantation annealing was achieved, as well as the effective removal of radiation-induced donor defects. In some samples, however, activation of acceptor-like defects not related to mercury vacancies as a result of annealing was observed, possibly related to the effect of the substrate.

1 Introduction

Ion implantation remains to be the most widely used method for fabrication of *p-n* junctions for photodiodes based on Hg$_{1-x}$Cd$_x$Te (MCT), the basic photoelectronics material in the infrared part of the spectrum. Nowadays, the most popular photodiode technique is based on the implantation of arsenic, with fabrication of a *p$^+$*-type implanted region in an *n*-type material. Dark currents in *p-n* junctions of the '*p$^+$–n*' type are believed to be substantially lower than those in '*n$^+$–p*'-type structures, which provides a higher working temperature or a longer wavelength cut-off sensitivity threshold of photodiodes [1-3]. This is due, among other things, to the fact that *n*-type MCT typically has lower concentration of deep levels which limit the minority carrier lifetime and thus, the performance of the photodetectors.

After arsenic implantation, the implanted MCT region typically has *n*-type conductivity and high density of radiation-induced structural defects. To achieve *p*-type conductivity, the number of the defects should be reduced and arsenic must be activated electrically. For this purpose, activation annealings are performed, but the best implantation and annealing strategy is yet to be found. For example, problems of arsenic activation were reported with the whole epitaxial structure sometimes converting into *p*-type conductivity after implantation and annealing [4].

The purpose of this work was to investigate defect structure of arsenic-implanted MCT films with the use of optical reflectance and Raman scattering as well as via studying the electrical properties of the films.

2 Experimental

In this study, we used Hg$_{1-x}$Cd$_x$Te epitaxial structures with composition (CdTe molar fraction) x ranging from 0.23 to 0.30. The structures were grown with molecular-beam epitaxy on Si (013) substrates with CdTe/ZnTe buffer layers [2] and had an "active' layer with constant x and a vary-band protective layer with composition at the surface approaching x=0.45. As-grown structures had *n*–type conductivity with electron concentration as measured at the temperature T=77 K n_{77}=(2.8–7.4)×10^{14} cm^{-3}. They were implanted with As$^+$ or As^{++} ions with E=190 keV or 350 keV energy, respectively, and 10^{14} cm^{-2} dose. After implantation, the structures were subjected to thermal activation annealing in saturated Hg vapors (360 °C, 2 h and 220 °C, 24 h).

Ion implantation was performed using IMC200 (Ion Beam Services, France) installation and arsenic profiles

---

* Corresponding author: mynkad@mail.ioffe.ru

were studied using Secondary-Ion Mass-Spectroscopy (Cameca IMS-6F, France).

Optical reflectance spectra were recorded in 300 to 800 nm wavelength range at T=300 K using Shimadzu UV-3600 (Japan) spectrometer.

Micro–Raman spectra were recorded at T=300 K in the spectral range 50–1300 cm^{-1} using Renishaw in Via Raman System with HeNe laser (wavelength 633 nm), a cooled CCD camera and an optical Leica microscope.

Electrical parameters of the films were determined with the measurements of the magnetic field dependence of the Hall coefficient R_H and conductivity σ at T=77 K. The dependences were analyzed using discrete mobility spectrum analysis (DMSA) method [5].

3 Results and Discussion

Figure 1 summarizes Secondary-Ion Mass-Spectroscopy (SIMS) data for the samples studied. As can be seen, experimental arsenic profiles could be grouped into two types, according to the implantation energy used. The experimental profiles could be well fitted with calculated ones obtained with the use of the TRIM software. Average concentration of implanted arsenic was estimated as N_{as}(avg) $=A_{As}/d_r$, where A_{As} is the area under the profile and d_r is implantation depth (0.3 µm for 190 keV ion energy and 0.5 µm for 350 keV ion energy). For E=190 and 350 keV, N_{as}(avg) was 3.7×10^{18} cm^{-3} and 2.2×10^{18} cm^{-3}, respectively.
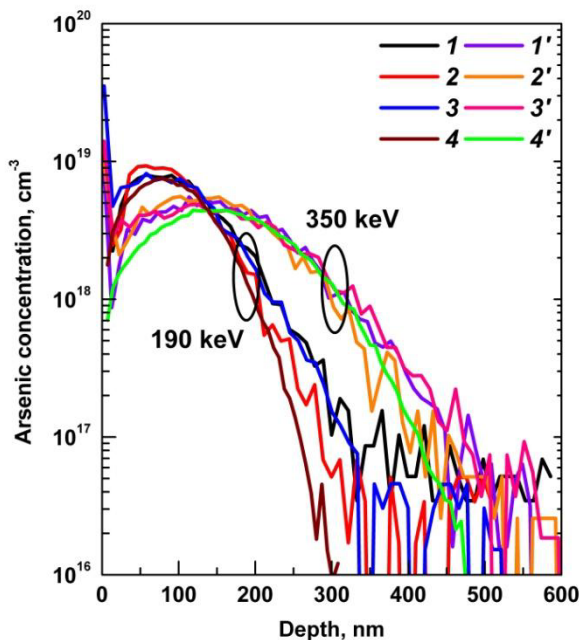

Fig. 1. Experimental arsenic profiles for samples with x=0.30, 0.23 and 0.29 (curves *1, 1'; 2, 2'* and *3, 3'* respectively), implanted with ion energy 190 keV (curves *1-3*) and 350 keV (curves *1'-3'*), respectively. Curves *4* and *4'* show the results of TRIM modelling.

Figure 2 shows optical reflectance spectra for the sample with x=0.30. It is known that in MCT optical reflectance spectra, there exists a typical doublet of E_1

and $E_1+\Delta_1$ peaks, which are due to transitions $\Lambda_{4,5} \rightarrow \Lambda_6$ and $\Lambda_6 \rightarrow \Lambda_6$, respectively. The position of the peaks provides information on the energy gap (composition x), while the shape of the peaks speaks of the structural perfection of the material [6]. It followed from the reflectance data obtained that the 'sharpness' of the peak E_1 was higher after implantation with As^{++} ions with E=350 keV than after implantation with As$^+$ ions with E=190 keV. This can be clearly seen in Figure 2, similar results were obtained for other samples. This meant that structural perfection at the surface was higher after implantation with more energetic ions.
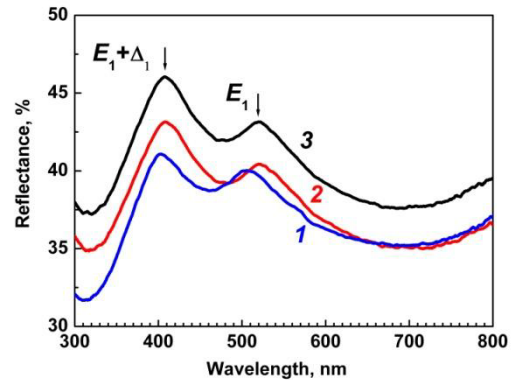

Fig. 2. Optical reflection spectra for the sample with x=0.30: as-grown sample (curve *1*), and samples after implantation with As^{++} 350 keV ions (curve *2*) and As$^+$ 190 keV ions (curve *3*).

For all the samples subjected to ion implantation and activation annealing, the chemical composition at the surface determined according to the position of the E_1 peak appeared to be smaller than that before activation annealing, thus, the annealing led to the enrichment of the surface vary-band protective layer with mercury.

These conclusions were confirmed with micro-Raman spectroscopy data (spectra not shown). According to the identification data available in the literature ([6-11]), typical Raman spectra of the as-grown samples contained lines which could be associated with TA$_2$, LA$_2$ (HgTe), LO$_1$ (CdTe) and LO$_2$ (HgTe) phonon modes and modes related to Te$_{Hg}$ and V_{Hg} defects and Te nanoinclusions. All the lines remained in the spectra of implanted samples with some re-distribution of intensities.

Figure 3 shows primary envelopes of mobility spectra for the studied sample with x=0.30. Shown are the envelopes for the as-grown sample, sample after ion implantation (energy 350 keV, dose 10^{14} cm^{-2}) and arsenic activation annealing, similar implanted and annealed sample after 1 µm of the surface layer was removed with chemical etching, and the same sample with extra 1.2 µm removed with the etching.

In the as-grown sample, conductivity was mostly determined by active-layer electrons with concentration $n_{77} \sim 3 \times 10^{14}$ cm^{-3} and low-mobility electrons of a transitional layer adjacent to the buffer layer. After implantation and annealing, conductivity increased from 0.36 up to 0.85 (Ohm·cm)$^{-1}$ and was now defined by heavy holes with mobility μ_h=110 cm^2/(V·s), and light

holes. High-mobility electrons of the active layer ceased to contribute to conductivity. This could be explained by formation of hole-type conductivity. After chemically removing $\Delta d_1 \sim 1$ μm, the set of carriers remained the same, however, concentration of heavy holes went down from 4×10^{16} cm^{-3} to 4.2×10^{15} cm^{-3}, while mobility increased from 110 up to 310 cm^2/(V·s), witnessing to removal of surface layer containing implanted (and activated) arsenic. The removal of extra 1.2 μm did not affect the parameters. Thus, in this case activation annealing led to conductivity type conversion across the whole thickness of the structure, which was due to generation of acceptors that most probably were not related to Hg vacancies. Similar observations related to activation, as a result of implantation and annealing, of yet not identified acceptors in MCT epitaxial films grown on Si were reported on the basis of photoluminescence studies performed on the material with $x \sim 0.4$ [4].
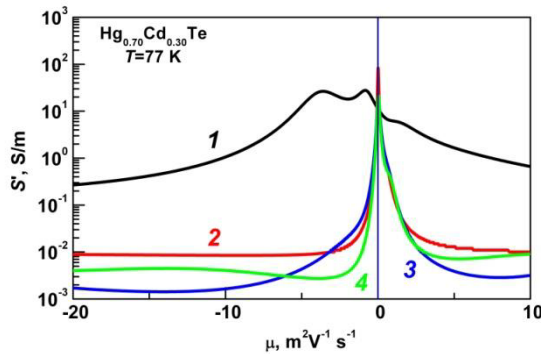

Fig. 3. Primary mobility envelopes for the sample with x=0.30: *1*, as-grown sample; *2*, sample after implantation and annealing; *3*, sample after 1 μm was removed with chemical etching; *4*, sample after extra 1.2 μm was removed with the etching.

Figure 4 shows primary envelopes of mobility spectra for the sample with x=0.23. Presented are the envelopes for the as-grown sample, sample after ion implantation (energy 350 keV, dose 10^{14} cm^{-2}) and arsenic activation annealing, similar implanted and annealed sample after 0.5 μm of the surface layer was removed with chemical etching, and the same sample after extra 0.9 μm was removed with the etching.

In as-grown sample conductivity σ was mostly determined by active-layer electrons with concentration $n_{77} \sim 8.6 \cdot 10^{14}$ cm^{-3} and low-mobility electrons of the transitional layer at the interface with the CdTe buffer layer, typical of such type of structures [2]. After implantation and annealing, σ decreased from 3.7 down to 2.8 (Ohm·cm)$^{-1}$ and was now defined by heavy holes with mobility μ_h=32 cm^2/(V·s), light holes and active-layer and transitional-layer electrons. This can be explained by formation of hole-type conductivity. After chemically removing $\Delta d_1 \sim 0.5$ μm, the set of carriers changed as heavy holes have gone: thus, the surface layer containing implanted (and activated) arsenic was removed. The removal of extra 0.9 μm-thick layer did not affect the parameters. Thus, activation annealing in

this case led to activation of implanted arsenic across the thickness of the implanted layer and also modified the properties of the rest of the active layer (which remained *n*-type). A similar result was obtained for the MCT sample with x=0.29.
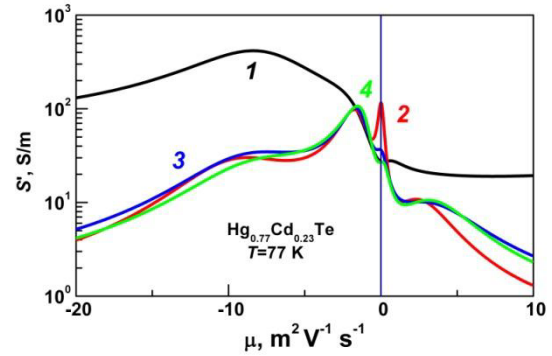

Fig. 4. Primary mobility envelopes for the sample with x=0.23: *1*, as-grown sample; *2*, sample after implantation and annealing; *3*, sample after 0.5 μm was removed with chemical etching; *4*, sample after extra 0.9 μm was removed with the etching.

On the basis of SIMS data and results of electrical measurements, we were able to make a comparison of 'real' heavy hole concentration in implanted layer $p_r = p_h \cdot \Sigma d / d_r$ with average arsenic ion concentration $N_{As}(avg)$ mentioned above. For example, for the sample with x=0.23 implanted with 350 keV ion energy, $p_r = p_h \cdot \Sigma d / d_r = 2.25 \times 10^{17} \times 8.3/0.5 = 3.74 \times 10^{18}$ cm^{-3}, where Σd is the total thickness of MCT film. $N_{As}(avg)$ for this sample was $2.2 \cdot 10^{18}$ cm^{-3}.

The results of the comparison are summarized in Table 1. As can be seen in this Table, heavy hole concentration in implanted layer agrees quite well with average arsenic ion concentration, with sample with x=0.29 implanted with 350 keV ion energy being the only exception. Thus, for these samples we can speak of 100% arsenic activation as a result of annealing.

Table 1. Electrical activation of the implanted arsenic.

x	0.23	0.23	0.29	0.29
Σd, μm	8.3	8.3	7.4	7.4
Ions	As$^+$	As^{++}	As$^+$	As^{++}
p_{77}, cm^{-3}	$9.3 \cdot 10^{16}$	$2.3 \cdot 10^{17}$	$1.8 \cdot 10^{17}$	$4.7 \cdot 10^{16}$
μ_{p77}, cm^2/(V·s)	66	32	19	77
p_{r77}, cm^{-3}	$2.6 \cdot 10^{18}$	$3.7 \cdot 10^{18}$	$4.4 \cdot 10^{18}$	$6.9 \cdot 10^{17}$
d_r, nm	300	500	300	500
$N_{As}(avg)$, cm^{-3}	$3.7 \cdot 10^{18}$	$2.2 \cdot 10^{18}$	$3.7 \cdot 10^{18}$	$2.2 \cdot 10^{18}$

4 Conclusions

In this work, the defect structure of arsenic-implanted HgCdTe films with the use of optical reflectance and Raman scattering as well as via studying the electrical properties of the films was investigated. The studies of optical reflection showed that the structural perfection of the samples remained higher after implantation of more energetic arsenic ions (350 keV vs 190 keV). In the samples with the composition of the active layer x=0.23 and x=0.29, as a result of implantation and activation annealing, a 'p^+–n'-type structure was formed. The concentration of heavy holes in implanted area reduced to the thickness of arsenic profile agreed quite well with the concentration of implanted ions. This spoke of 100% of activation of implanted ions as a result of annealing. Indeed, in this case activation annealing also removed radiation-induced defects of donor type.

In the sample with x=0.30, the annealing led to the formation of a 'p^+–p'-type structure. The conductivity type conversion throughout the whole thickness of the structure in this case was most probably caused by the generation (activation) of acceptor-like defects not related to mercury vacancies.

Generally, optical reflectance, micro-Raman studies and electrical measurements were shown to provide highly detailed characteristics of the implanted structures based on MCT.

References

1. L. Mollard, G. Bourgeois, C. Lobre, S. Gout, S. Viollet-Bosson, N. Baier, G. Destefanis, O. Gravrand, J.P. Barnes, F. Milesi, J. Electron. Mater. **43**, 802 (2014)
2. M.V. Yakushev, V.S. Varavin, V.G. Remesnik, D.V. Marin, Semiconductors **48**, 767 (2014)
3. A.M. Itsuno, P.Y. Emelie, J.D. Phillips, S. Velicu, C.H. Grein, P.S. Wijewarnasuriya, J. Electron. Mater. **39**, 945 (2010)
4. K.D. Mynbaev, N.L. Bazhenov, M.V. Yakushev, D.V. Marin, V.S. Varavin, Yu.G. Sidorov, S.A. Dvoretsky, Tech. Phys. Lett. **40**, 708 (2014)
5. V.V. Bogoboyashchyy, A.I. Elizarov, I.I. Izhnin, Semicond. Sci. Technol. **20**, 726 (2005)
6. S.A. Dvoretsky, N.N. Mikhailov, V.G. Remesnik, N.Kh. Talipov, Avtometriya **5**, 73 (1998) (in Russian)
7. A.I. Belogorokhov, I.A. Denisov, N.A. Smirnova, L.I. Belogorokhova, Semiconductors **38**, 84 (2004)
8. A.I. Belogorokhov, N.A. Smirnova, I.A. Denisov, L.I. Belogorokhova, B.N. Levonovich, Phys. Stat. Sol. C **7**, 1624 (2010)
9. I. Hill, J. Appl. Phys. **67**, 4270 (1990)
10. S.H. Shih, J. Bajai, L.A. Moudy, D.T. Cheung, Appl. Phys. Lett. **43**, 68 (1983)
11. A. Tverjanovich, K. Rodionov, E. Bychkov, J. Sol. State Chem. **190**, 271 (2012)